

SplatFace: Gaussian Splat Face Reconstruction Leveraging an Optimizable Surface

Jiahao Luo¹, Jing Liu², and James Davis¹

¹ University of California, Santa Cruz CA 95064, USA

² ByteDance Inc, San Jose CA 95110, USA
jluo53@ucsc.edu

Abstract. We present SplatFace, a novel Gaussian splatting framework designed for 3D human face reconstruction without reliance on accurate pre-determined geometry. Our method is designed to simultaneously deliver both high-quality novel view rendering and accurate 3D mesh reconstructions. We incorporate a generic 3D Morphable Model (3DMM) to provide a surface geometric structure, making it possible to reconstruct faces with a limited set of input images. We introduce a joint optimization strategy that refines both the Gaussians and the morphable surface through a synergistic non-rigid alignment process. A novel distance metric, splat-to-surface, is proposed to improve alignment by considering both the Gaussian position and covariance. The surface information is also utilized to incorporate a world-space densification process, resulting in superior reconstruction quality. Our experimental analysis demonstrates that the proposed method is competitive with both other Gaussian splatting techniques in novel view synthesis and other 3D reconstruction methods in producing 3D face meshes with high geometric precision.

Keywords: 3D face reconstruction · 3D Gaussian Splatting · Novel view synthesis

1 Introduction

Human face models are used extensively in a variety of domains, such as 3D avatars [41], biometric recognition [4], photo editing [31], and the movie industry [5]. Historically, the production of high-quality 3D facial models has required multi-view images and specialized equipment and setups [5, 8]. Recent research has achieved impressive reconstruction results given just a few images, primarily through the integration of regression networks with a 3D Morphable Model (3DMM) [1, 2, 11, 27, 40]. However, mesh-based 3DMM face reconstruction focuses on geometric accuracy, often at the expense of photometric quality, ignoring complex scene elements and light interaction.

With the advent of Neural Radiance Fields (NeRF) [21], facial capture has witnessed substantial progress. Geometry-aware NeRF-based methods have demonstrated their effectiveness in capturing complex facial movements [39] and rendering extrapolated views [23]. The introduction of 3D Gaussian Splatting (3DGS)

[15] shows considerable promise in tackling the dual challenges of achieving complex scene fidelity and speeding up both training and rendering. It employs an explicit, yet adaptive, representation [42] combined with differentiable rendering. Despite these advancements, NeRF and Gaussian splatting methods typically require either a substantial number of multi-view inputs such as video sequences and multi-view captures, or robust and accurate geometry guidance such as pre-determined and scene specific 3D depth information. These prerequisites can pose limitations in practical applications where such data is difficult to obtain. A method which requires only a few input images and no precise depth information would expand the range of circumstances in which face reconstruction is possible.

In this work, we introduce SplatFace, a novel Gaussian splatting framework designed for 3D human face reconstruction without the reliance on accurate pre-determined geometry. Our framework aims to simultaneously deliver high-quality novel view rendering and a precise mesh-based reconstruction. To achieve this, we incorporate a generic 3D Morphable Model (3DMM) for geometric guidance, allowing reconstruction with only a limited set of input images. We propose to jointly optimize Gaussians and the morphable model surface. This is achieved through a non-rigid alignment process that tightly integrates both components. We propose a novel splat-to-surface distance metric that enhances alignment by considering both Gaussian centers and their covariances. In addition, we augment the view-space adaptive densification technique of 3DGS, with world-space densification, capitalizing on the presence of the surface to enhance results. Our experimental evaluation demonstrates that the proposed method outperforms existing techniques in terms of both novel view synthesis image fidelity and 3D face mesh geometric accuracy.

2 Related Work

2.1 Few Shot 3D Face Reconstruction

Realistic 3D human face reconstruction from a few 2D images has a long history of active research. Amazing results have been achieved with explicit representations such as meshes or depth maps [9, 11, 13, 16, 17, 19, 20, 27, 29]. Typically 3D morphable face model parameters [3] are regressed by training an encoder-decoder network [26, 37]. There also exists work that directly regresses 3D geometries [14, 18, 25]. However, explicit representations face challenges in modeling complex scene elements such as hair, clothes or highly anisotropic surfaces. Neural radiance field (NeRF) [21] based representations have also been used to represent a dynamic human head and body [12, 22, 23, 39]. Our work is directly inspired by this line of research, however we address few shot face reconstruction in the context of 3D Gaussian Splatting [15].

2.2 Gaussian Splatting and Point Based methods for Avatars

The pursuit of real-time animatable volumetric avatar systems has been a challenging goal in virtual human research. PointAvatar [36] proposed a deformable

point-based representation that achieves efficient training and re-rendering, even in new environments. 3D Gaussian Splatting [15] has been quickly embraced by the community to build more efficient and animatable avatar systems [6, 10, 24, 30, 34]. Unfortunately, these methods require hundreds or thousands of multi-view frames of the target subject as input, in order to reconstruct a high fidelity avatar to animate. In our work, we focus on dramatically reducing the number of input frames required to accurately reconstruct the subject’s face using 3D Gaussian Splatting.

Similar to our work, GaussianAvatars [24] proposes a technique for creating head avatars by constraining 3D Gaussians to a parametric morphable face mesh model. However, this is achieved via a binding inheritance strategy where each Gaussian is attached explicitly to the surface and constrained within an associated parent triangle. In contrast, our method allows greater flexibility in splat position, but provides more constraint on splat covariance. Their work also uses video input with an order of magnitude more input frames than our work, seeking to produce an animatable model. Our work focuses on introducing methods suitable when only a few viewpoints are available.

2.3 Few Shot Gaussian Splatting Reconstruction

Despite the success of Gaussian Splatting in representing complex scenes, it remains a difficult problem to synthesize novel viewpoints when only a few input images are available. This condition is often called few-shot reconstruction and is difficult due to inherent ambiguities in learning 3D structure from a limited set of 2D images. Several methods based on Gaussian Splatting have been proposed to address the general scene few-shot reconstruction problem [7, 28, 38]. These methods leverage a pre-trained depth estimation model to extrapolate pseudo input views to assist the reconstruction process. Chung et al. [7] add a depth map loss term together with a depth smoothness term to regularize the optimization process. SparseGS [28] further incorporates a generative diffusion model to refine the pseudo input views, improving floater pruning and overall synthesis quality. FSGS [38] pairs depth regularization with a proximity-guided Gaussian unpooling process to enhance scene coverage and reconstruction.

These methods estimate a geometry prior in a pre-processing step which remains static during splat optimization, and use this prior primarily to constrain splat position. In contrast we use a geometry prior which is jointly optimized with the Gaussian splats, and is additionally used to guide both splat orientation and splat densification.

3 Method

The overall pipeline of our proposed method, SplatFace, is shown in Figure 1. One key idea in our work is to insert an optimizable morphable surface which moves together with the Gaussian splats. The splats and surface are initialized using the same template surface across different identities. In contrast to 3DGS

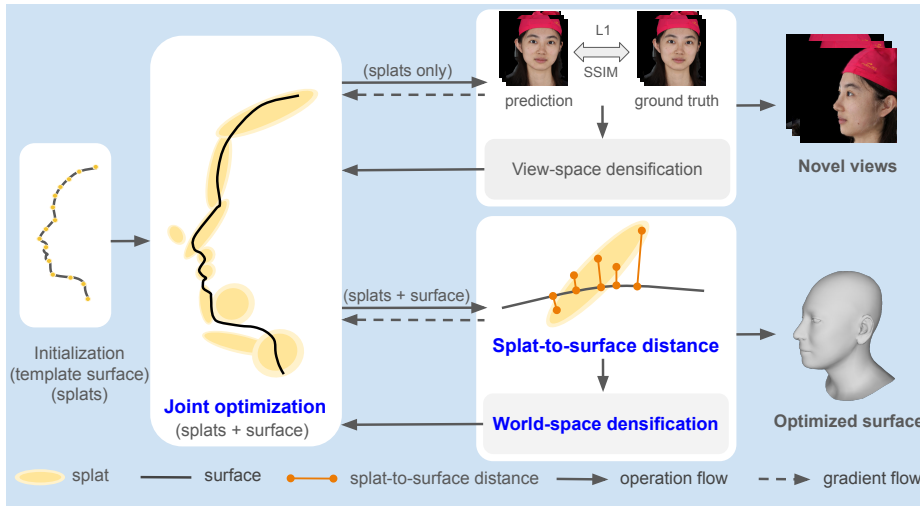


Fig. 1: Diagram of overall process: SplatFace begins by initializing 3D Gaussians and a surface using the template mesh derived from a 3D Morphable Model (3DMM). The Gaussians and surface are then simultaneously refined through a *joint optimization* process. Splats are constrained by image photoconsistency, and by a novel *splat-to-surface distance* metric. This measure is introduced to accurately quantify the discrepancies between the Gaussian splat distribution and the surface, considering both the position and covariance of the Gaussians. Additionally, the presence of a surface allows the introduction of *world-space densification*. As a result of this overall process, we obtain both enhanced novel view synthesis and a finely-tuned 3D mesh.

that focuses mainly on view-space operations and image similarity (the upper box showing operation and gradient flow), we propose a parallel process that focuses on world-space operations (the lower box showing operation and gradient flow). We propose *joint optimization* of the Gaussians and surface using a *splat-to-surface distance* metric, as well as *world-space densification* to capture high-frequency details without generating extra floating splats. This process results in both a Gaussian splat model for novel view synthesis and an accurate 3D mesh representation of the surface. After a very brief introduction to Gaussian splatting, we provide a detailed presentation of each novel component in the subsequent sections.

3.1 Background on Gaussian Splatting

Gaussian splatting [15] represents a 3D scene as a set of 3D Gaussian primitives with adaptive covariances, and renders an image using volume splatting. This model requires neither normal nor triangulation. Each Gaussian splat is defined by a full 3D covariance matrix Σ centered at its position in the object space:

$$G(\mathbf{x}) = e^{-\frac{1}{2}(\mathbf{x}-\boldsymbol{\mu})^T \Sigma^{-1}(\mathbf{x}-\boldsymbol{\mu})}. \quad (1)$$

Covariance matrices have physical meaning only when they are positive semi-definite. Gradient descent cannot be easily constrained to produce such valid matrices. Instead of directly optimizing the covariance matrix Σ to obtain 3D Gaussians that represent the radiance field, we follow previous research [42] and approximate the covariance matrix with scaling and rotation:

$$\Sigma = RSS^T R^T. \quad (2)$$

To render images from new views, the color of a pixel is obtained by projecting and rasterizing Gaussian splats followed by alpha blending. Color of each splat is modeled with a view-dependent term using the following function:

$$c = \sum_{j=1}^n c_j \alpha_j \prod_{j=1}^{i-1} (1 - \alpha_j), \quad (3)$$

where α_i and c_i are the opacity and a spherical harmonic representation of color computed for each Gaussian splat.

For a more detailed description of Gaussian splatting we refer readers to prior research. Due to limited space, in this paper we focus on introducing and evaluating the novel contributions of our work.

3.2 Joint Optimization of Gaussian Splats and Geometric Surface

Our method results in a face reconstruction supporting novel view synthesis and producing a precise 3D geometric model. We propose a joint optimization between Gaussian splatting and a constrained surface model representing the 3D geometry of a human face. This joint optimization is in contrast to existing work which relies on a pre-determined depth estimate from monocular depth prediction [28, 38], multi-view stereo [23], or head tracking [10, 34].

We adopt a 3D morphable model (3DMM) [18] as a generic representation of the face surface. This model is widely used in face reconstruction research so we do not discuss the details here. The morphable model is initialized to the mean face (identity parameters set to zero). Gaussians are initialized using this generic surface template, with the initial scale, rotation, and color set to zero. During training, the Gaussians change and move according to photo-consistency with target images, but also follow a loss term for distance and orientation relative to the surface. The surface itself follows a loss which constrains it to lie near the position of Gaussian splats.

In order to prevent overfitting, we regularize the surface more strongly in early iterations of optimization, relaxing the regularization in later stages to allow better detail capture. The 3D morphable model representation has far fewer parameters than Gaussian splats, so is efficient to optimize. We combine the shape, expression and pose parameters along with the Gaussians in the joint optimization.

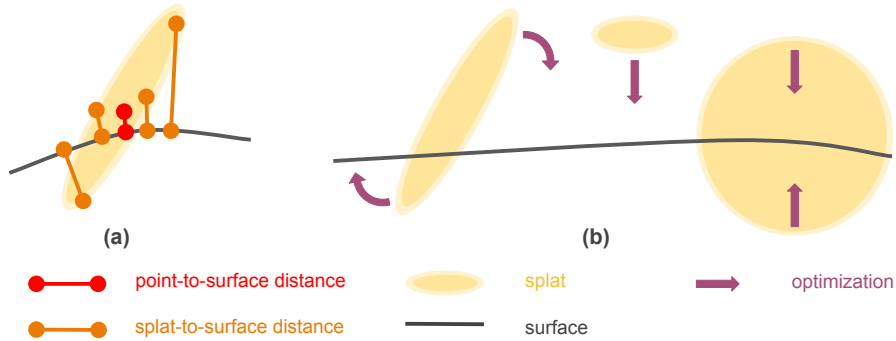


Fig. 2: (a) Illustration of splat-to-surface distance and (b) the modifications to splats this distance is meant to encourage. Point-to-surface distance, shown in red, ignores covariance and considers each splat as a point. The point-to-surface distance will only calculate distance from splat center to the surface. In contrast, splat-to-surface distance accounts for the extended nature of the Gaussian distribution. Minimizing splat-to-surface distance will simultaneously optimize the orientation, position and scale of Gaussian Splats.

3.3 Splat-to-Surface Distance

A key contribution of our work is using an explicit surface model which allows us to introduce a splat-to-surface distance measure. This distance can be used to enforce an additional loss during optimization intended to encourage splats positioned on the surface, rather than positioned away from the surface. From training viewpoints, splats away from the surface may be effective at representing image variation, but from alternate viewpoints these splats are perceived as floating away from the surface. This problem is exacerbated when only a few viewpoints are available during training since insufficient image photoconsistency constraints exist to ensure placement consistent with actual scene geometry.

To encourage Gaussians aligned with the surface, we introduce a term to minimize a distance function between the splats and the surface. Point-to-surface distance is the most commonly used distance functions to align point clouds to surfaces, and has been widely used in morphable model fitting and Iterative Closest Point (ICP). This measure is also known as point-to-face and point-to-plane. Given a point in the point cloud, point-to-surface distance is defined as the distance between the point and its closest triangle on the surface. Unfortunately, this widely used measure is designed for points with no spatial extent. Gaussian splats have a covariance matrix which defines a scale, and a more complex measure of distance is needed.

Figure 2(a) shows a splat positioned near to the surface. The splat position is indicated in red and the point-to-surface distance is the distance from its position (geometric center) to the surface, shown with a red bar. However, given a splat with scaling and rotation, a small distance between the splat center and the

surface is not sufficient to guarantee a good alignment. In the example shown, some portions of the splat extend a considerable distance from the surface. To illustrate this point, several other positions sampled from the Gaussian distribution are shown with their distance to the surface shown with orange bars. When a splat is oriented as shown in this visualization it will lead to “spiky” artifacts when new views are rendered away from training viewpoints.

To address this difficulty it is necessary to define a new distance measure which encourages splats not to extend too far from the surface. Figure 2(b) shows the desired behavior. Splats should be encouraged to rotate, move towards the surface, and reduce size in the direction perpendicular to the surface.

We propose a novel *splat-to-surface* distance to correctly measure the distance between a splat distribution and the surface. Splat-to-surface distance can be calculated as the integral of the point-to-surface distance over the 3D Gaussian distribution as:

$$\int_{\mathbf{x} \sim G(\mathbf{x})} G(\mathbf{x}) |(\mathbf{x} - \mathbf{x}_i) \cdot \mathbf{n}_i|, \quad (4)$$

where \mathbf{x} represent a position within the distribution. \mathbf{x}_i is the corresponding point on the closest triangle, and \mathbf{n}_i is the unit normal at \mathbf{x}_i . Making an assumption of local surface planarity, the dot product is the point-to-surface distance of each position within the Gaussian. $G(\mathbf{x})$ is the 3D Gaussian distribution value defined in formula 1 which serves as the weights of each point-to-surface distance.

Since this distance measure must be estimated efficiently during optimization, we approximate the integral with random sampling. We sample from each splat’s Gaussian distribution N times, and calculate the average of the sampled distances:

$$\sum_{\mathbf{x}_j \sim G(\mathbf{x})}^N \frac{1}{N} |(\mathbf{x}_j - \mathbf{x}_i) \cdot \mathbf{n}_i|, \quad (5)$$

where \mathbf{x}_j is one of the N samples.

3.4 World-space densification

World-space densification uses the surface model to augment view-space densification with a new geometry based policy. Floating splats that lie off the surface are a known difficulty in Gaussian splatting. While view-space densification helps mitigate the difficulty when many views are available, the problem remains in scenarios where only a few input views are available. With few views there are insufficient photoconsistency constraints to trigger densification. The spherical harmonic parameters which encode color are intended to allow enough variation to encode shading variation, but with a small number of views they can also encode floating splats that project to different surface points in different views. We

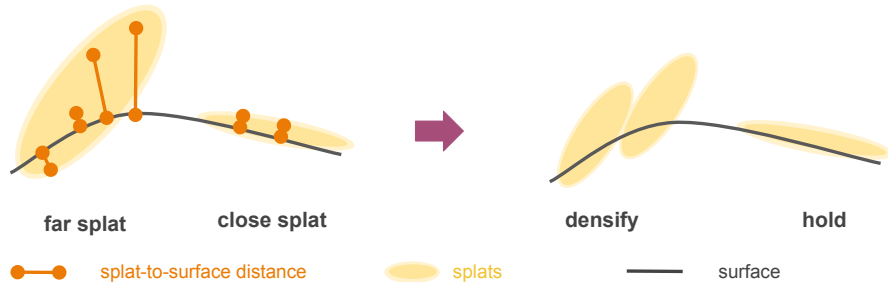


Fig. 3: World-space densification. We densify splats that are far from the surface using the proposed splat-to-surface distance. Gaussians with any sampled points far from the surface are considered far and either split or cloned. This helps generate multiple splats closer to the surface which are more expressive than a single floating or spiky splat which extends far from the surface.

have observed that the Gaussian model tends to use floaters to represent high-frequency details such as eyebrow. In the training view, overlapping floaters can capture high-frequency details and generate a low loss in the RGB domain.

It would be possible to increase the weight of the splat-to-surface loss to force all splats to lie very near the surface. However in regions like eyebrows this results in over-regularization. It is important to allow some variation and expressiveness since the true geometry of hair is closer to volumetric. We have empirically found that some floating splats do not induce RGB constraints in training views, so will not trigger densification. In addition, more splats better match the required expressiveness of high-frequency details.

Based on these empirical observations, we densify splats which are far from the surface. Fig 3 illustrate how world space densification works. We calculate the splat-to-surface distance and then we select those with any samples further than an adaptive threshold τ_{s2s} to densify. We use the same densification techniques including clone and split from 3DGS. Splats which lie closer than the threshold distance are not densified by this rule, although they may be densified by view-space densification if they have a large accumulated RGB gradient. In addition to helping the splats better represent the input views, more splats in regions of complexity help the jointly optimized surface model to better capture the details of face shape.

3.5 Combined loss function

We optimize Gaussian splat parameters and morphable model parameters jointly with a total loss defined as:

$$loss = \lambda_{rgb} loss_{rgb} + \lambda_{s2s} loss_{s2s} + \lambda_{reg} loss_{reg}, \quad (6)$$

where $loss_{rgb}$ is a combination of L1 and SSIM measuring RGB consistency on training views. This loss term is the same as vanilla 3DGS. $loss_{s2s}$ is our proposed splat-to-surface distance (Equation 5), bringing splats and surface into alignment. We calculate $loss_{s2s}$ only in the face region since this is the only region in which the face model is valid. $loss_{reg}$ is a regularization term constraining surface shape to prevent overfitting. In order to facilitate a fair comparison, we modify only the loss terms, leaving all other aspects of optimization identical to the baseline 3DGS implementation.

4 Implementation, Results, and Evaluation

4.1 Implementation

Datasets We evaluate our method on two datasets, FaceScape [32] and ILSH [35]. The FaceScape dataset contains high-resolution light-stage images captured by DSLR cameras on hundreds of identities. Each capture contains about 50 images with viewing angles spaced approximately 20 degree away from each other. The FaceScape dataset also provide 3D meshes, with reported reconstruction error less than 0.3mm. We randomly select 10 identities to evaluate both on 3D face mesh reconstruction and novel view synthesis. The ILSH dataset include high-resolution light-stage capture from 24 cameras on 52 identities. We randomly select 10 identities to evaluate novel view synthesis.

Experimental Setting We downsample all DSLR images by a factor of four (1086x724 in the FaceScape and 1024x750 in the ILSH dataset). We generate masks to remove background regions, and adopt dynamic background color. We adopt all hyper parameters of vanilla 3DGS for a fair comparison. We train our proposed method with 10k iteration, taking about 10 minutes on a Nvidia RTX 3080.

4.2 Comparison on novel view synthesis

Figure 4 presents a qualitative visual comparison between our method and several baseline methods, including 3DGS [15], Mip-splatting [33] and FSGS [38]. We compare on both the FaceScape and ILSH datasets, using 5 images as input. We show an evaluation on both a near and far test viewpoint. In the first row of each individual, we show a test view near to one of the training views. 3DGS and Mip-splatting tend to produce noisy results, whereas FSGS often yields overly smoothed outcomes. In contrast, our method succeeds in capturing high-frequency details with minimal artifacts. In the second row for each test subject, we show an example which is far from the training views. Extrapolation of viewpoint away from training views is very challenging and we do not expect perfect results from any method. 3DGS and Mip-Splatting produce noisy results and exhibit floating splats due to the lack of geometric constraints. These floating splats are most visible in profile views since they lie obviously away from

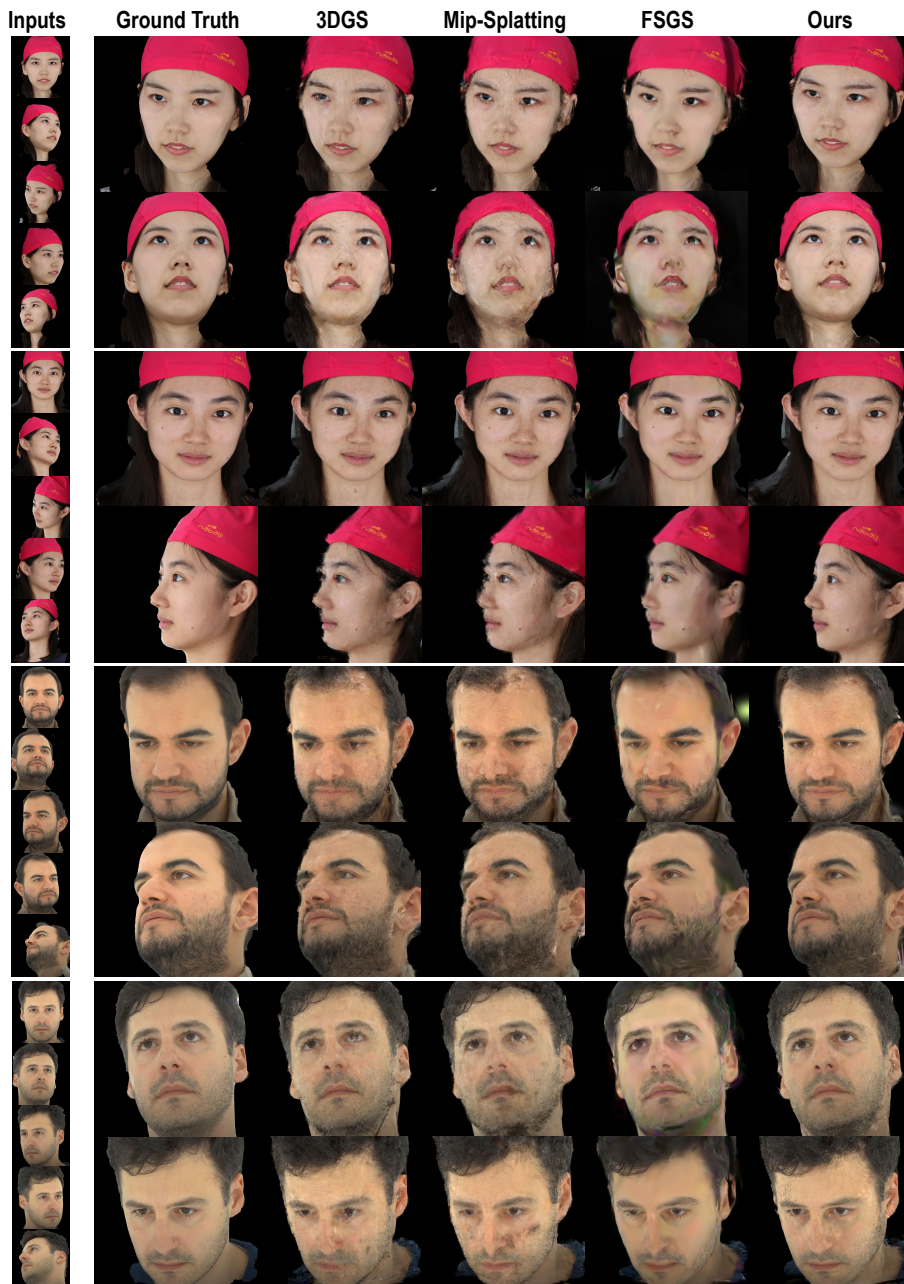


Fig. 4: Qualitative comparison on novel view synthesis. We compare our results with other Gaussian splatting methods on the FaceScape [32] and ILSH [35] datasets. Each method uses 5-view input images, shown on the left. For each individual, a test view that is close to the training views is shown in the top row, and a test view further from the training images is shown in the bottom row. Our method produce results with fewer artifacts than the comparison methods.

the face. FSGS results in mismatched colors and poor geometry, stemming from the use of a non-optimizable prior that lacks the precision necessary to properly constrain splat placement. While our method also contains artifacts, it yields the most visually appealing novel view synthesis.

Table 1 presents a quantitative comparison of image error in terms of L1, SSIM, PSNR and LPIPS on each dataset. Our method outperforms the comparison set of methods. Reported numbers are averaged across multiple views and across all test subjects in each dataset.

Methods	FaceScape				ILSH			
	L1 ↓	SSIM ↑	PSNR ↑	LPIPS ↓	L1 ↓	SSIM ↑	PSNR ↑	LPIPS ↓
3DGS [27]	0.0273	0.8350	25.34	0.1404	0.0405	0.7277	22.04	0.2224
Mip-Splatting [2]	0.0436	0.8387	25.60	0.1379	0.0447	0.6826	22.18	0.2406
FSGS [1]	0.0349	0.8307	24.27	0.2950	0.0492	0.7064	21.33	0.3535
Ours	0.0233	0.8556	26.58	0.1193	0.0391	0.7459	22.70	0.1871

Table 1: Quantitative results on the FaceScape and ILSH datasets, using the L1, SSIM, PSNR and LPIPS image quality metrics. All metrics show that our method achieves better performance than the comparison Gaussian splatting methods.

4.3 Comparison on surface mesh reconstruction

Joint optimization of Gaussian splats *and* 3D morphable model parameters results in a 3D mesh which estimates surface geometry. This 3D geometry is useful beyond view synthesis and many methods exist specifically to estimate 3D face shape from images. In order to evaluate our results, we compare with four state-of-the-art (SOTA) multi-view 3D face reconstruction methods: MVF-Net [27], DFNRMVS [2], INORig [1] and HRN [17] using the FaceScape dataset. HRN [17] uses geometry disentanglement and introduces a hierarchical representation. MVF-Net [27] and DFNRMVS [2] train convolutional neural networks to explicitly enforce multi-view appearance consistency. All of these methods focus on mesh generation, seeking to minimize 3D surface error rather than image based errors common in novel view synthesis. Since most of the comparison methods use 3 input views, we do the same for fair comparison.

For error analysis, the predicted meshes from each method are aligned to ground truth using the Iterative Closest Point (ICP) algorithm. For each point on the ground truth scan, we calculate the point-to-face distance in millimeters by finding the closest triangle in the predicted mesh. From this set of distances, we calculate summary statistics like mean-squared error (MSE), Median, and a robust approximation of maximum error which discards 10% of high error points as outliers (M90).

Table 2 presents a quantitative comparison of our method against the state of the art dedicated 3D face estimation methods. Our method outperforms the comparisons on all error metrics.

Methods	MSE ↓	Median ↓	M90 ↓
MVF-Net [27]	1.75	1.45	3.60
DFNRMVS [2]	1.73	1.40	3.56
INORig [1]	1.46	1.18	3.05
HRN [17]	1.28	0.96	2.54
Ours	1.06	0.85	2.21

Table 2: Quantitative comparison of face shape estimation with state of the art methods using the FaceScape dataset. Geometric error in millimeters is provided using MSE, Median, and max error after rejecting 10% outliers (M90). Our method outperforms existing few-view 3D face reconstruction methods.

4.4 Ablation study

Surface initialization	Surface optimization	L1 ↓	SSIM ↑	PSNR ↑	LPIPS ↓
No surface	×	0.0273	0.8350	25.34	0.1404
Template	×	0.0245	0.8495	25.79	0.1259
Template	✓	0.0233	0.8556	26.58	0.1193
Ground truth	✓	0.0233	0.8716	26.68	0.1243

Table 3: Ablation study showing the value of joint optimization and the acceptability of our surface initialization. A jointly optimized template surface results in higher quality images than the ablation conditions of no surface constraint or a non-optimized template surface. Initialization with a generic template surface reaches similar image quality to initialization with the ground truth surface, indicating that optimization is able to adequately refine the surface representation.

Effectiveness of joint optimization and initialization Our method jointly optimizes Gaussian splats and surface geometry parameters. Since splat locations are constrained by the surface, there is a concern that the surface might converge to an incorrect estimate of face shape and inadvertently drag the Gaussian splats to incorrect locations, degrading performance. To evaluate this concern we test our method both while holding the surface estimate constant and while allowing joint optimization. Table 3 provides a quantitative comparison of results using L1, SSIM, PSNR, and LPIPS as performance measures. As shown in the first three rows of the table, having a template surface estimate improves the rendered image quality compared to having no surface estimate, but jointly optimizing the splats and surface leads to even greater accuracy.

We initialize the surface prior to a template mesh representing the average face. This prior is only approximate initially, but is jointly optimized to find a high quality estimate of 3D face shape. Nevertheless, there may be residual shape error which affects splat placement and thus image rendering. To assess

the impact of using an approximation during surface initialization, we compare against using the ground truth face shape. The final two rows of Table 3 provide this comparison. Initialization with a template mesh produces renderings nearly as high quality as using a ground truth mesh for the surface. This indicates that our method is not very sensitive to initialization conditions, and thus using a simple template mesh is justified.

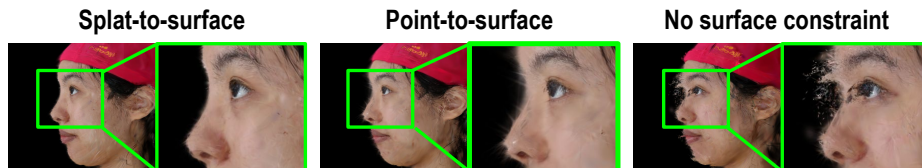


Fig. 5: Visual ablation study on splat-to-face distance. When no surface constraint is present, many splats float away from the face surface. A simple point-to-surface constraint is effective in moving these splats to lie near to the surface, however the lack of an orientation constraint results in many “spiky” artifacts. Our splat-to-surface distance offers better alignment between splats and surface, resulting in fewer spiky artifacts in far test views.

Point-to-surface distance	Splat-to-surface distance	World-space densification	L1 ↓	SSIM ↑	PSNR ↑	LPIPS ↓
×	×	×	0.0273	0.8350	25.34	0.1404
✓	×	×	0.0243	0.8492	26.14	0.1293
✓	×	✓	0.0237	0.8492	26.38	0.1249
×	✓	×	0.0239	0.8477	26.47	0.1243
×	✓	✓	0.0233	0.8556	26.58	0.1193

Table 4: Quantitative ablation study on splat-to-surface distance and world-space densification. The proposed splat-to-surface distance metric results in higher image quality than than the ablation conditions of no surface constraint and a simple point-to-surface constraint. Incorporating world-space densification further refines performance. The highest image quality is obtained when using both of our enhancements.

Effectiveness of splat-to-surface distance and world space densification

The existence of a surface prior allows a splat-to-surface distance loss term as well as world space densification. We perform an ablation study to demonstrate the importance of these terms to our method.

Table 4 presents novel view synthesis accuracy quantitatively, with and without our proposed components. Minimizing a distance function between splats and an optimizable surface enhances performance across all evaluation metrics.

When contrasted with simple point-to-surface distance, our splat-to-surface approach exhibits superior improvement. We evaluated world space densification using both point-to-surface and splat-to-surface distance functions. Densification results in quantitative improvements in both cases.

Visual examples are perhaps better than numbers at illustrating *why* splat-to-surface is effective. Figure 5 illustrates the visual impact of our method. The chosen test view is positioned at an angle greater than 40 degrees from any of the five training views. This is too far for high quality reconstruction, but emphasizes the artifacts that appear even at closer angles. In the absence of geometric surface constraints, errant points (floaters) not attached to the face surface are visible. Using a simple point-to-surface distance measure successfully pulls these floaters back towards the surface, however it fails to provide any constraint on the orientation and scale of the splats. As a result many splats are incorrectly oriented away from the surface, producing “spikes” sticking out of the face. Using a splat-to-surface distance measure helps orient the splats, dramatically reducing spikes.

5 Limitations

Our method aligns Gaussians to the surface, which can lead to over-regularization in regions where the surface model lacks the necessary expressiveness. Typical examples include complex geometries like teeth, facial hair and accessories. In addition, our method only applies to scenes for which an optimizable surface models exist. We focus on faces in this work, and fall back to vanilla 3D Gaussian Splatting (3DGS) in non-face regions like hair and body. Finally, while our method outperforms existing Gaussian splatting methods on both near and far test views, the rendered images are not yet completely free of artifacts. Achieving cleaner rendering, especially on far test views, remains a challenge.

6 Conclusion

In summary, we present SplatFace, an advancement in 3D human face reconstruction technology, which is particularly suited to the few-view input scenario. This method avoids the need for precise predefined geometry, and instead jointly optimizes Gaussian splats and a morphable surface model. A splat-to-surface distance function and world-space densification serve to reduce artifacts caused by the limited number of input views. The method outputs both a Gaussian splatting model suitable for rendering novel viewpoints, and a 3D surface mesh suitable for traditional graphics pipelines including modeling and animation. Both of these outputs have been experimentally validated as higher accuracy than existing state of the art methods which focus on only one of the two goals.

References

1. Bai, Z., Cui, Z., Liu, X., Tan, P.: Riggable 3D face reconstruction via in-network optimization. In: Proceedings of the IEEE/CVF Conference on Computer Vision and Pattern Recognition. pp. 6216–6225 (2021)
2. Bai, Z., Cui, Z., Rahim, J.A., Liu, X., Tan, P.: Deep facial non-rigid multi-view stereo. In: Proceedings of the IEEE/CVF Conference on Computer Vision and Pattern Recognition. pp. 5850–5860 (2020)
3. Blanz, V., Vetter, T.: A morphable model for the synthesis of 3D faces. In: Proceedings of the 22nd annual conference on Computer graphics and interactive techniques. pp. 351–358 (1995)
4. Blanz, V., Vetter, T.: Face recognition based on fitting a 3D morphable model. *IEEE Transactions on Pattern Analysis and Machine Intelligence* **25**(9), 1063–1074 (2003)
5. Borshukov, G., Piponi, D., Larsen, O., Lewis, J.P., Tempelaar-Lietz, C.: Universal capture-image-based facial animation for "the matrix reloaded". In: ACM Siggraph 2005 Courses, pp. 16–es (2005)
6. Chen, Y., Wang, L., Li, Q., Xiao, H., Zhang, S., Yao, H., Liu, Y.: Monogaussianavatar: Monocular gaussian point-based head avatar. arXiv preprint arXiv:2312.04558 (2023)
7. Chung, J., Oh, J., Lee, K.M.: Depth-regularized optimization for 3d gaussian splatting in few-shot images. arXiv preprint arXiv:2311.13398 (2023)
8. Debevec, P., Hawkins, T., Tchou, C., Duiker, H.P., Sarokin, W., Sagar, M.: Acquiring the reflectance field of a human face. In: Proceedings of the 27th Annual Conference on Computer Graphics and Interactive Techniques. pp. 145–156 (2000)
9. Deng, Y., Yang, J., Xu, S., Chen, D., Jia, Y., Tong, X.: Accurate 3D face reconstruction with weakly-supervised learning: From single image to image set. In: Proceedings of the IEEE/CVF Conference on Computer Vision and Pattern Recognition Workshops. pp. 0–0 (2019)
10. Dhamo, H., Nie, Y., Moreau, A., Song, J., Shaw, R., Zhou, Y., Pérez-Pellitero, E.: Headgas: Real-time animatable head avatars via 3d gaussian splatting. arXiv preprint arXiv:2312.02902 (2023)
11. Feng, Y., Feng, H., Black, M.J., Bolkart, T.: Learning an animatable detailed 3D face model from in-the-wild images. *ACM Transactions on Graphics (ToG)* **40**(4), 1–13 (2021)
12. Gao, X., Zhong, C., Xiang, J., Hong, Y., Guo, Y., Zhang, J.: Reconstructing personalized semantic facial nerf models from monocular video. *ACM Transactions on Graphics (TOG)* **41**(6), 1–12 (2022)
13. Gecer, B., Ploumpis, S., Kotsia, I., Zafeiriou, S.: Ganfit: Generative adversarial network fitting for high fidelity 3D face reconstruction. In: Proceedings of the IEEE/CVF Conference on Computer Vision and Pattern Recognition. pp. 1155–1164 (2019)
14. Guo, J., Zhu, X., Yang, Y., Yang, F., Lei, Z., Li, S.Z.: Towards fast, accurate and stable 3D dense face alignment. In: Computer Vision–ECCV 2020: 16th European Conference, Glasgow, UK, August 23–28, 2020, Proceedings, Part XIX. pp. 152–168. Springer (2020)
15. Kerbl, B., Kopanas, G., Leimkühler, T., Drettakis, G.: 3d gaussian splatting for real-time radiance field rendering. *ACM Transactions on Graphics* **42**(4) (July 2023), <https://repo-sam.inria.fr/fungraph/3d-gaussian-splatting/>

16. Kumar, R., Luo, J., Pang, A., Davis, J.: Disjoint pose and shape for 3d face reconstruction. In: Proceedings of the IEEE/CVF International Conference on Computer Vision. pp. 3115–3125 (2023)
17. Lei, B., Ren, J., Feng, M., Cui, M., Xie, X.: A hierarchical representation network for accurate and detailed face reconstruction from in-the-wild images. Proceedings of the IEEE/CVF Conference on Computer Vision and Pattern Recognition (2023)
18. Li, T., Bolkart, T., Black, M.J., Li, H., Romero, J.: Learning a model of facial shape and expression from 4d scans. *ACM Trans. Graph.* **36**(6), 194–1 (2017)
19. Luo, J., Khan, F.H., Mori, I., de Silva, A., Ruezga, E.S., Liu, M., Pang, A., Davis, J.: How much does input data type impact final face model accuracy? In: Proceedings of the IEEE/CVF Conference on Computer Vision and Pattern Recognition. pp. 18985–18994 (2022)
20. Luo, J., Ruezga, E.S., Davis, J.: How accurate is passive stereo for 3D face reconstruction? In: 2022 IEEE International Conference on Image Processing (ICIP). pp. 2516–2520. IEEE (2022)
21. Mildenhall, B., Srinivasan, P.P., Tancik, M., Barron, J.T., Ramamoorthi, R., Ng, R.: Nerf: Representing scenes as neural radiance fields for view synthesis. *Communications of the ACM* **65**(1), 99–106 (2021)
22. Park, K., Sinha, U., Barron, J.T., Bouaziz, S., Goldman, D.B., Seitz, S.M., Martin-Brualla, R.: Nerfies: Deformable neural radiance fields. ICCV (2021)
23. Prinzler, M., Hilliges, O., Thies, J.: Diner: Depth-aware image-based neural radiance fields. In: Proceedings of the IEEE/CVF Conference on Computer Vision and Pattern Recognition. pp. 12449–12459 (2023)
24. Qian, S., Kirschstein, T., Schoneveld, L., Davoli, D., Giebenhain, S., Nießner, M.: Gaussianavatars: Photorealistic head avatars with rigged 3d gaussians. arXiv preprint arXiv:2312.02069 (2023)
25. Sanyal, S., Bolkart, T., Feng, H., Black, M.J.: Learning to regress 3D face shape and expression from an image without 3D supervision. In: Proceedings of the IEEE/CVF Conference on Computer Vision and Pattern Recognition. pp. 7763–7772 (2019)
26. Tuan Tran, A., Hassner, T., Masi, I., Medioni, G.: Regressing robust and discriminative 3D morphable models with a very deep neural network. In: Proceedings of the IEEE conference on Computer Vision and Pattern Recognition. pp. 5163–5172 (2017)
27. Wu, F., Bao, L., Chen, Y., Ling, Y., Song, Y., Li, S., Ngan, K.N., Liu, W.: Mvf-net: Multi-view 3D face morphable model regression. In: Proceedings of the IEEE/CVF Conference on Computer Vision and Pattern Recognition. pp. 959–968 (2019)
28. Xiong, H., Muttukuru, S., Upadhyay, R., Chari, P., Kadambi, A.: Sparsegs: Real-time 360° sparse view synthesis using gaussian splatting. Arxiv (2023)
29. Xu, S., Yang, J., Chen, D., Wen, F., Deng, Y., Jia, Y., Xin, T.: Deep 3d portrait from a single image. In: Proceedings of the IEEE Conference on Computer Vision and Pattern Recognition (CVPR) (2020)
30. Xu, Y., Chen, B., Li, Z., Zhang, H., Wang, L., Zheng, Z., Liu, Y.: Gaussian head avatar: Ultra high-fidelity head avatar via dynamic gaussians. arXiv preprint arXiv:2312.03029 (2023)
31. Yang, F., Wang, J., Shechtman, E., Bourdev, L., Metaxas, D.: Expression flow for 3D-aware face component transfer. In: ACM SIGGRAPH 2011 papers, pp. 1–10 (2011)
32. Yang, H., Zhu, H., Wang, Y., Huang, M., Shen, Q., Yang, R., Cao, X.: Facescape: A large-scale high quality 3D face dataset and detailed riggable 3D face prediction.

- In: IEEE/CVF Conference on Computer Vision and Pattern Recognition (CVPR) (June 2020)
33. Yu, Z., Chen, A., Huang, B., Sattler, T., Geiger, A.: Mip-splatting: Alias-free 3d gaussian splatting. arXiv preprint arXiv:2311.16493 (2023)
 34. Zhao, Z., Bao, Z., Li, Q., Qiu, G., Liu, K.: Psavatar: A point-based morphable shape model for real-time head avatar creation with 3d gaussian splatting. arXiv preprint arXiv:2401.12900 (2024)
 35. Zheng, J., Jang, Y., Papaioannou, A., Kampouris, C., Potamias, R.A., Papantoniou, F.P., Galanakis, E., Leonardis, A., Zafeiriou, S.: Ilsh: The imperial light-stage head dataset for human head view synthesis. In: Proceedings of the IEEE/CVF International Conference on Computer Vision. pp. 1112–1120 (2023)
 36. Zheng, Y., Yifan, W., Wetzstein, G., Black, M.J., Hilliges, O.: Pointavatar: Deformable point-based head avatars from videos. In: Proceedings of the IEEE/CVF Conference on Computer Vision and Pattern Recognition (CVPR) (2023)
 37. Zhu, X., Lei, Z., Liu, X., Shi, H., Li, S.Z.: Face alignment across large poses: A 3D solution. In: Proceedings of the IEEE Conference on Computer Vision and Pattern Recognition. pp. 146–155 (2016)
 38. Zhu, Z., Fan, Z., Jiang, Y., Wang, Z.: Fsgs: Real-time few-shot view synthesis using gaussian splatting (2023)
 39. Zielonka, W., Bolkart, T., Thies, J.: Instant volumetric head avatars. 2023 IEEE/CVF Conference on Computer Vision and Pattern Recognition (CVPR) pp. 4574–4584 (2022), <https://api.semanticscholar.org/CorpusID:253761096>
 40. Zielonka, W., Bolkart, T., Thies, J.: Towards metrical reconstruction of human faces. In: European Conference on Computer Vision. pp. 250–269. Springer (2022)
 41. Zollhöfer, M., Martinek, M., Greiner, G., Stamminger, M., Süßmuth, J.: Automatic reconstruction of personalized avatars from 3D face scans. *Computer Animation and Virtual Worlds* **22**(2-3), 195–202 (2011)
 42. Zwicker, M., Pfister, H., Van Baar, J., Gross, M.: Surface splatting. In: Proceedings of the 28th annual conference on Computer graphics and interactive techniques. pp. 371–378 (2001)